

NUMERICAL INVESTIGATION OF HYPERSONIC WALL-BOUNDED SHEAR FLOWS – PART 1: EFFUSION COOLING

Jens Linn & Markus J. Kloker

*Institut für Aerodynamik und Gasdynamik, Universität Stuttgart
Pfaffenwaldring 21, 70550 Stuttgart, Germany*

linn@iag.uni-stuttgart.de

Abstract

Direct numerical simulations (DNS) are carried out to study the laminar stability properties of an effusion-cooled adiabatic flat-plate boundary layer at Mach 6. Through four aligned rows of holes, cold gas is blown into the boundary layer at the wall and background disturbances are excited at the wall upstream of the holes. Two cases are compared, with small and large spanwise spacing of the holes. Despite strong localized vortex-like flow deformations in both cases no strong “secondary” instability sets in. From studies of incompressible cases it is known that wall blowing can strongly destabilize the boundary layer. Thus an “incompressible” reference case (Mach 0.6) is simulated and compared with the effusion-cooled Mach-6 case. Differences are found indicating that the high Mach number has a stabilizing effect on the young effusion-cooled boundary layer.

1 Introduction

For aerospace or hypersonic cruise vehicle the state of the boundary layer is of great importance because for turbulent boundary layers the thermal loads and skin friction are higher than in laminar boundary layers. Therefore, knowledge of cooling features and laminar-turbulent transition is necessary for the design and the thermal protection system (TPS). Different strategies are used to reduce the thermal loads of hypervelocity vehicles, e.g. radiation, ablation, transpiration or effusion cooling.

The subject of this paper is the effusion or film cooling at wind tunnel conditions, where cold air is blown into an adiabatic Mach-6 boundary layer through spanwise rows of holes. This implies a change in the laminar stability properties of the boundary.

2 Numerical Method

The numerical method is based on the complete 3-d unsteady compressible Navier-Stokes equations in a conservative formulation. The equations are solved in a rectangular integration domain on a flat plate, which does not contain the shock wave induced by the leading edge. In streamwise (x -) and wall-normal (y -) direction the discretization is realized by compact finite differences of 6th order [6]. In the spanwise (z -) direction, the flow is assumed to be periodic, thus a Fourier spectral representation is employed. The time integration is done with a

classical 4th-order Runge-Kutta method. A detailed description of the algorithm and boundary conditions is reported in [1,3].

Effusion cooling is modelled by prescribing a wall-normal mass flux $(\rho v)_c$ and wall temperature T_c distribution over the hole (figure 1) with a polynomial of 5th order [7]. In the adiabatic case only $T_{c,core}$ at the hole center is fixed.

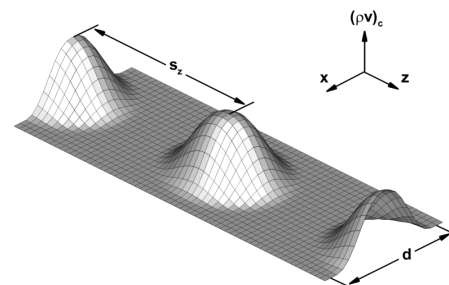


Figure 1: $(\rho v)_c$ -distribution at the wall for on row of holes.

3 Results

Here we investigate an adiabatic Mach-6 boundary layer in which cold air is blown through four aligned rows of holes. The freestream temperature is $T_\infty^* = 89\text{K}$ ($\approx 1/7 \cdot T_{rec}^*$) and the pressure is $p_\infty^* = 0.0038\text{bar}$, matching the flow parameters of experiments in the hypersonic wind tunnel H2K of DLR-Köln [2]. Thus, with $Re_L = 10^5$, the reference values for nondimensionalisation are $L^* = 36.28\text{ mm}$, $u_\infty^* = 1134.8\text{ m/s}$, and $Re_{unit} = 2.8 \cdot 10^5$. Non dimensional values are without asteriks, see also table 1. We look at two cases with different spanwise spacing s_z of the holes. The hole region reaches from $Re_x = 2.2 \cdot 10^5$ to $2.75 \cdot 10^5$. In case **A** the holes have a small spanwise spacing $s_{z,A} = 3 \cdot d_c$ (hole diameter - $d_c = 0.055 \approx 0.56 \cdot \delta_c$), in contrast to case **B** where the spanwise spacing is enlarged ($s_{z,B} = 12 \cdot d_c$). The cooling gas temperature is $T_{c,core}^* = 1/2 \cdot T_{rec}^*$, the blowing ratio $(\rho v)_c^* / (\rho v)_\infty^* = 0.15$, and the hole diameter d_c is in both cases equal. Thus the integral massflow through the holes per spanwise unit is in case **B** only one quarter of case **A**. Investigations based on the primary Linear Stability Theory (LST) have shown (see, e.g. [8]) that wall cooling stabilises 1st-mode (vorticity) disturbances and destabilises 2nd-mode (acoustic) disturbances.

A crosscut of the u -velocity and temperature field downstream of the rows is shown in figures 2a) and 2b).

In case **B** (right), the boundary layer is deformed much stronger than in case **A** (left; mushroom like structures). From the holes, counter-rotating longitudinal vortex pairs (CVPs) emerge which are along the jet trajectory and have such a rotation sense that fluid is transported away from the wall in the streamwise hole center line. However, the CVPs of both cases decay downstream.

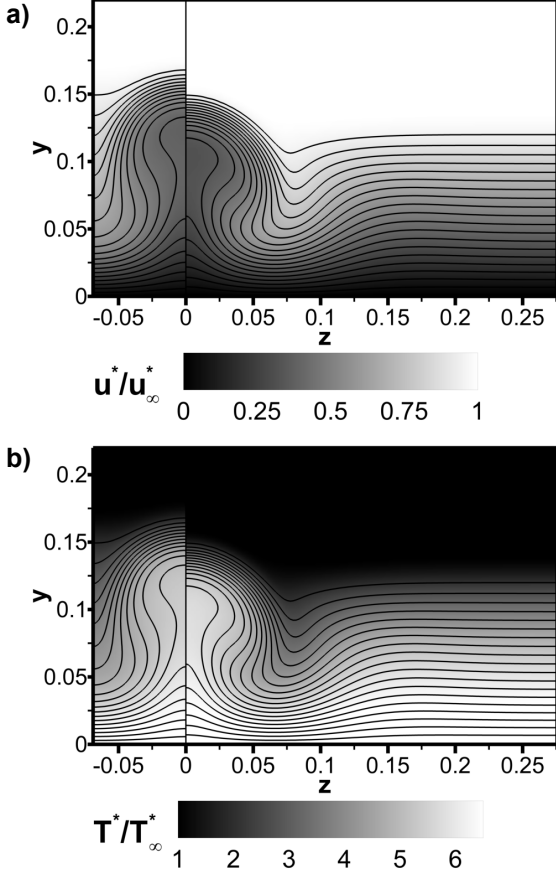


Figure 2: u -velocity iso-contours in a crosscut (half the respective spanwise domain width is shown) at $Re_x = 3.12 \cdot 10^5$ downstream of the holes for case **A** (left) and case **B** (right); $0.05 \leq u \leq 1$, $\Delta u = 0.05$. a) with u -shading and b) temperature shading.

Upstream of the holes, unsteady 2-d disturbance waves are generated at $Re_x = 1.78 \cdot 10^5$ for a bunch of frequencies to check for laminar instability. Note that, due to the large steady vortices, 3-d unsteady disturbances are nonlinearly generated with the 2-d packet.

Figure 3 shows the downstream development of the u -disturbance amplitudes (u'_h – maximum over y and z) from a timewise Fourier analysis for both cases. The curve (0,0) represents the timewise and spanwise mean flow deformation of the 2-d boundary layer. In case **A** (0,0) is stronger than in case **B** due to the higher injected massflow per spanwise unit and the 3-d deformation is less, resulting in an approximately equal level of the curve $\omega = 0$ that includes both effects. All frequencies are damped or are neutral for $Re_x > 5 \cdot 10^5$, except frequencies near $\omega = 10$, being also amplified in the pure 2-d base flow as a 2nd mode. Here, however, it is a

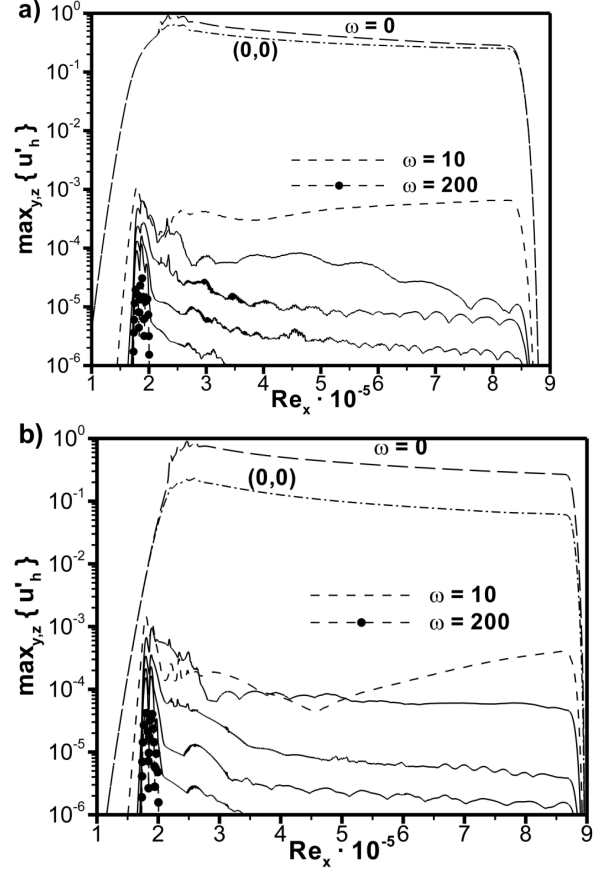


Figure 3: Downstream disturbance-amplitude development for both cases (**A** – small spanwise spacing, **B** – large spanwise spacing; $\omega=10$ is $f^* = \omega u^*_{\infty} / (2\pi L^*) = 49.78$ kHz).

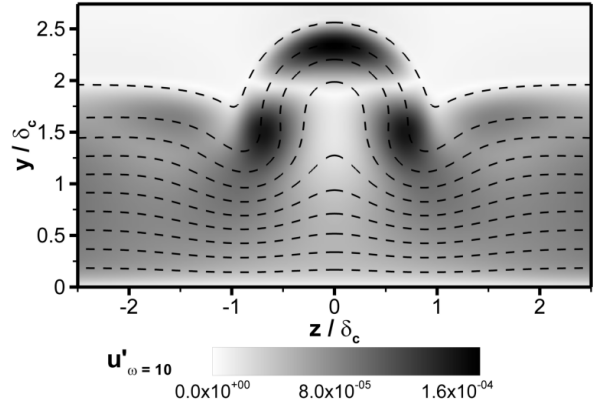


Figure 4: Amplitude distribution (shaded) and mean flow (isolines) at $Re_x = 6.5 \cdot 10^5$ for case **B**; $0.1 \leq u \leq 1$, $\Delta u = 0.1$.

disturbance localized in the y - z plane as a localized secondary mode (figure 4). In case **B** this frequency is amplified much stronger, despite a reduced receptivity. Low frequencies are neutral or damped like in case **A** (we checked down to $\omega=1$). Thus the steady 3-d flow deformation by blowing does not invoke sudden transition in the young boundary layer in the front part of the plate. A small spanwise hole spacing is preferable due to larger

cooling effectiveness and lower amplification of unsteady disturbances.

	Low M-case C	Case B
M_∞	0.6	6.0
T_∞^*	290 K	89 K
u_∞^*	204.8 m/s	1135.8 m/s
p_∞^*	1.0 bar	0.0038 bar
L^*	7.25 mm	36.28 mm
Re_{unit}	$13.8 \cdot 10^6$ 1/m	$2.8 \cdot 10^6$ 1/m
Re_L	10^5	10^5
Wall condition	adiabatic	adiabatic
T_{rec}^*	307.6 K	629 K
$T_{c,core}^*$	290 K	293 K
v_c^*/u_∞^*	0.15	0.45
d_c/λ_z	0.105	0.105

Table 1: Parameters of the Mach-0.6 (**C**) and Mach-6 case (**B**).

From investigations of incompressible boundary layers it is known that blowing often strongly destabilizes the boundary layer. Thus a Mach-0.6 case (**C**) is simulated and compared with case **B** to clarify the effects. We chose an equal $R_x=469.57 = Re_x^{1/2}$ at the first row of holes in both cases. Table 1 summarizes the simulation parameters. The Mach-0.6 case **C** has a five times larger unit Reynolds number Re_{unit} due to the smaller ($\approx 1/27$) kinematic viscosity. Furthermore we chose equal length scales ratios in both cases ($s_x/\delta_c = \text{const.}$; $s_z/\delta_c = \text{const.}$; $d/\delta_c = \text{const.}$) and equal blowing ratios $(\rho v)_c^*/(\rho v)_\infty^*=0.15$.

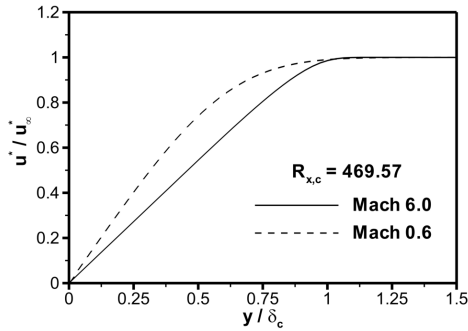


Figure 5: Comparison of u-velocity baseflow profiles at $R_x=469.57 (= Re_x^{1/2})$ without blowing for the two different Mach numbers.

In figure 5 the u-velocity profiles of the baseflow at the position of the first row of hole is shown. The wall gradient $\partial u/\partial y|_w \cdot \delta_c$ in the Mach-0.6 case is larger than in the Mach-6 case. With increasing Mach number, the skin friction and thus $\partial u/\partial y$ at the wall decreases.

A crosscut of the u-velocity field is shown in figure 6 at three boundary-layer thicknesses downstream of the last row of holes. In case **C**, we did not obtain a steady solution, due to self-excited unsteadiness of the boundary layer at the fourth hole row. Therefore in figure 6 the time mean of the u-velocity field is shown. The deformation of the boundary layer in case **C** is stronger than in the other case and closer to the wall due to the different

blowing velocity. It is in the Mach-6 case **B** three times larger than in the Mach-0.6 case **C**, due to the different effusion densities ($\rho_{Mach-0.6} \approx 1$; $\rho_{Mach-6} \approx 1/3$).

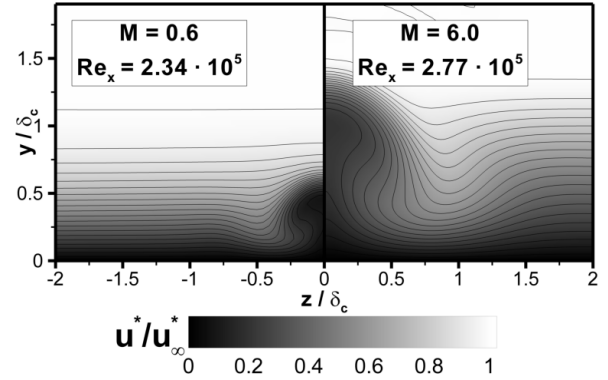


Figure 6: Visualisation of the u-velocity field in a crosscut at three boundary-layer thicknesses downstream the last row of holes.

In figure 7 the gradients $\partial u/\partial y$ and $\partial u/\partial z$ are shown in the same crosscut as in the previous figure. The gradients in the low Mach number case (**C**) are much larger than in case **B** due to the blowing. Furthermore the maximum of the gradients lay closer to the wall in case **C**. We note that, for a free shear layer, the dimensional disturbance growth rate is proportional to $\partial u/\partial y \cdot (u_\infty^*/L^*)$, the expression in brackets being almost equal for the two cases.

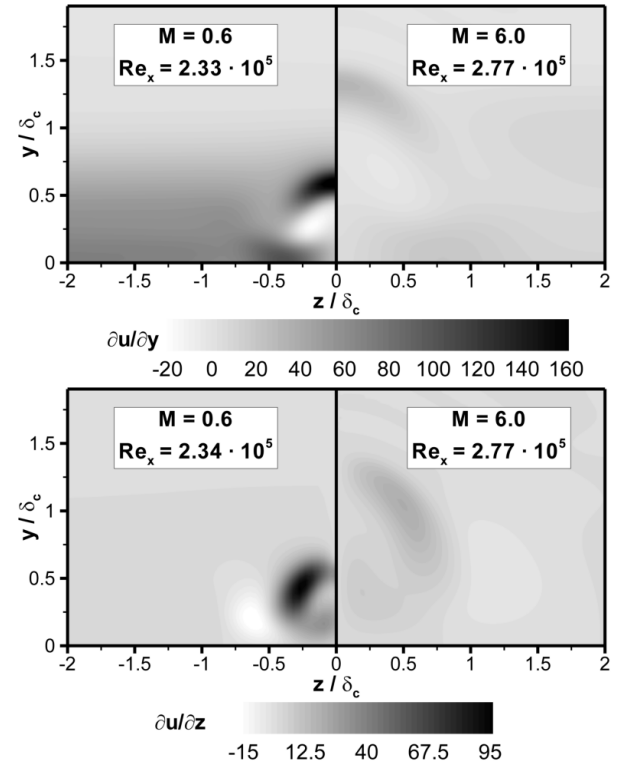


Figure 7: Contour plot of $\partial u/\partial y$ (upper figure) and $\partial u/\partial z$ (lower figure) in a crosscut behind the holes for cases **C** (left) and **B** (right).

The vortical structures (λ_2 -criterion, [5]) are shown in figure 8. In the Mach-0.6 case (snapshot) downstream travelling Λ vortices are directly generated by blowing at

the fourth hole row. This is in contrast to the Mach-6 case, where only a pair of steady longitudinal vortices is generated at each hole that decays downstream.

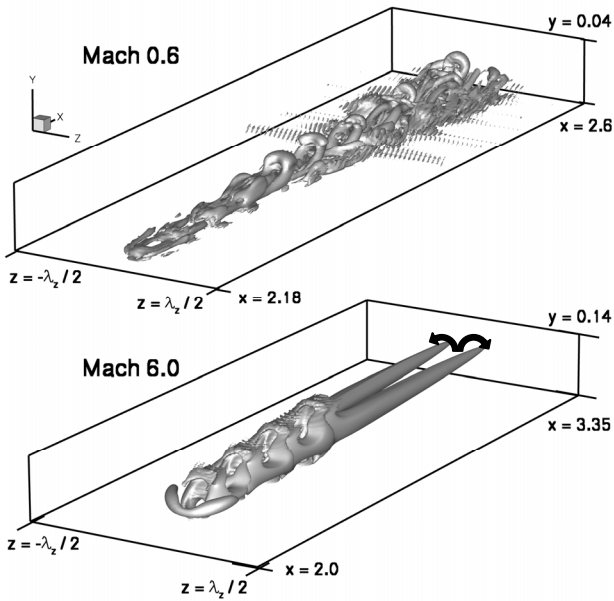


Figure 8: Visualisation of the vortical structures via λ_2 -isosurfaces for the Mach-0.6 (case **C**, snapshot) and Mach-6 case (case **B**). 42 or 85 spanwise harmonics have been computed.

4 Conclusion

In this paper we investigate the laminar instability of an adiabatic effusion-cooled Mach-6 boundary layer with four aligned row of holes and different spanwise hole spacings. We observe no transition at Mach 6, i.e. no explosive “secondary” instability of the mushroom-like structures generated by the vortices. The results show a destabilisation effect only with large spanwise spacing. In a low Mach-number reference case (Mach 0.6) self-excited unsteadiness by strong growth of background disturbances occurs. In this case Λ -vortices are generated at the last hole row, travelling downstream. The low Mach-number case has a stronger wall shear $\partial u / \partial y|_w$ and also stronger shear maxima $\partial u / \partial y|_{\max}$ in the longitudinal-cut plane and $\partial u / \partial z|_{\max}$ in the wall-parallel plane due to the deformation by blowing than the Mach-6 case. For effusion cooling a small spanwise spacing is preferable, not only because of the lower destabilisation effect but also of the larger cooling effectiveness.

Acknowledgements

The partial financial support of this work by the Helmholtz-Gemeinschaft (HGF) within project A8 of the RESPACE (Key Technologies for Reusable Space Systems) group is gratefully acknowledged. We thank the Höchstleistungsrechenzentrum Stuttgart (HLRS) for provision of supercomputing time and technical support within the project “LAMTUR”.

References

- [1] A. Babucke, J. Linn, M. Kloker, U. Rist, Direct numerical simulation of shear flow phenomena on parallel vector computers, In *High Performance Computing on Vector Systems* (ed. M. Resch & el.), Proc. High Performance Computing Center Stuttgart, Springer, pp. 229-247, 2003.
- [2] M. Bierbach, Untersuchungen zur aktiven Kühlung der Grenzschicht an einem Plattenmodell, Diplomarbeit, Technische Universität Darmstadt, 2005.
- [3] W. Eißler, H. Bestek, Spatial numerical Simulations of linear and weakly nonlinear wave instabilities in supersonic boundary layers, *Theoret. Comput. Fluid Dynamics*, vol. 8, pp. 219-235, 1995.
- [5] J. Jeong, F. Hussain, On the identification of a vortex, *J. Fluid Mech.*, vol.285, pp.69-94, 1995.
- [6] M. Kloker, A robust high-resolution split-type compact FD-scheme for spatial direct numerical simulation of boundary-layer transition, *Applied Scientific Research*, vol. 59, pp. 353-377, 1998.
- [7] J. Linn, M.J. Kloker, Numerical investigations of effusion cooling in hypersonic boundary-layer flow, In *New Results in Numerical and Experimental Dynamics VI* (ed. S. Jakirlic, C. Tropea, H.-J. Heinemann, R. Hilbig), NNFM, vol. 96, Springer, 2007.
- [8] M.R. Malik, Prediction and control of transition in supersonic and hypersonic boundary layers, *AIAA-Journal*, vol. 27, pp 1487-1493, 1989.